České vysoké učení technické v Praze
Fakulta elektrotechnická

Czech Technical University in Prague
Faculty of Electrical Engineering

doc. Dr. Ing. Jan Kybic

Registrace obrazů s aplikacemi v lékařství a biologii

Image registration and its biomedical applications

Summary

Image registration is one of the key tasks for biomedical imaging algorithms, the other being preprocessing, reconstruction, segmentation and classification. The input to image registration is two or more images and the goal is to find a geometrical transformation relating coordinates of corresponding locations in input images, The input can be also 3D volumes, sequences of 2D images, or sequences of 3D volumes; the images can be scalar or multichannel.

In biomedical imaging, image registration is often represented as a minimization problem. We specify a region of interest, an image similarity criterion such as a sum of squared differences or a mutual information, the class of allowable transformations such as rigid, affine, B-splines or unconstrained, and the regularization criterion such as the norm of the derivatives. The minimum of the criterion can be found by iterative multidimensional minimization such as gradient descent, Levenberg-Marquardt, or BFGS, and methods based on discrete labeling, such as GraphCut or message passing. The speed and robustness can be improved by multiresolution.

The applications of images registration include deformation and motion compensation and analysis, multi-subject analysis, image sequence analysis, fusing information from several images, change detection, motion modeling, elastography, 3D reconstruction from 2D slices or projections.

Sometimes all image pixels need not be considered. Images of linear branching structures such as blood vessels or nerve fibers can be advantageously registered by first matching the geometrical graphs. Other images can be registered through their segmentations. The uncertainty of image registration results can be determined be bootstrap resampling.

We will conclude with a few thoughts about biomedical imaging research in general and at CTU, and its future.

Souhrn

Registrace obrazů je jedním za základních problémů řešených v oblasti zpracování biomedicínských obrazů; ostatními jsou předzpracování, rekonstrukce, segmentace a klasifikace. Vstup do registračního algoritmu jsou dva nebo více obrazy a cílem je najít geometrickou transformaci mezi souřadnicemi odpovídajících si bodů ve vstupních obrazech. Vstupem mohou být i 3D obrázky nebo sekvence a může být i vícekanálový.

V biomedicínském zobrazování je registrace často reprezentována jako minimalizační problém. Zvolíme kritérium podobnosti obrazů jako je součet čtverců rozdílů nebo vzájemná informace. Zvolíme třídu transformací, např. euklidovské nebo reprezentovatelné B-spliny. Regularizace může penalizovat vysoké hodnoty derivací. Minimum kritéria je nalezeno iterativními algoritmy jako je gradientní sestup, BFGS, nebo Levenberg-Marquardt, nebo algoritmy pro diskrétní značkování jako je GraphCut nebo message passing. Robustnost může být vylepšena zpracováním ve více měřítcích.

Aplikace registrace zahrnují kompenzaci a analýzu deformace a pohybu, analýzu více subjektů, analýzu obrazových sekvencí, fúzi několika obrazů, detekci změn, elastografii nebo 3D rekonstrukci.

Někdy není potřeba zpracovávat všechny pixely. Obrázky s lineárními, grafům podobnými strukturami, jako jsou tepny a žíly nebo nervová vlákna, lze zaregistrovat tak, že nejdříve najdeme korespondence mezi těmito strukturami. Jiné obrázky mohou být zaregistrovány ze svých segmentací. Nejistota registrace může být odhadnuta metodou bootstrap.

Práci uzavřeme několika úvahami o výzkumu v oblasti biomedicínského zobrazování na ČVUT a jeho budoucnosti.

Klíčová slova: registrace obrazů, lékařství, biologie, zobrazovací metody, algoritmy

Keywords: image registration, medicine, biology, imaging methods, algorithms

Contents

Chapter 1

Introduction

The first part of the biomedical imaging chain is an acquisition device such as microscopy, MRI, CT or ultrasound, that converts physical properties of the subject or object being examined into multidimensional and often multichannel data. have become a standard part of both clinical and research procedures in medicine as well as in biology. The resolution keeps increasing and the dimensionality has changed from 2D to 3D and even to 4D, considering time. In many cases, human expert analysis of the data is impractical due to the amount of data to be analyzed. Hence, there is a strong need for automatic methods.

We will briefly review the main tasks for biomedical imaging algorithms in Chapter 2, before approaching our main subject, image registration, in Chapter 3. I have chosen to use for illustration my own work or the work of my students and collaborators, whenever possible.

The role of biomedical imaging algorithms is to process the data coming from the acquisition device to obtain the human-viewable image data, and to analyze it further to extract useful measurements or features, which should lead to a diagnostic decision in medicine or a hypothesis being proven in biology.

Biomedical imaging algorithms use many techniques from numerical mathematics, computer vision, machine learning and related disciplines. However, many of these methods need to be adapted to the particularities of the task or the imaging modalities such as high dimensionality, nonlinear deformations, appearance differences, lack of suitable feature points, lack of training data etc.

Chapter 2

Biomedical Imaging Algorithms

The most important tasks for biomedical imaging algorithms are preprocessing, reconstruction, segmentation, classification, and registration (addressed in Chapter 3).

2.1 Reconstruction

Some acquisition techniques produce raw data, which needs to be processed in order to obtain an image. An example is computed tomography, where an image is reconstructed from projections using filtered backprojection or other algorithms. In magnetic resonance imaging, an image is reconstructed by taking a Fourier transform of the acquired k-space data. *Parallel MRI* uses N coils with varying spatial sensitivity to increase the acquisition speed N times. Our reconstruction method PROBER uses B-splines [33] to achieve better signal to noise ratio than standard methods SENSE and GRAPPA. Another example is the spatio-temporal reconstruction of neuronal activity from the measurement of the electric potential and magnetic field on the head surface using EEG and MEG, respectively, where we have contributed an accurate forward model using a boundary element method [29, 30, 32].

2.2 Segmentation

The task of the segmentation is to divide the image into spatially coherent regions (classes) according to given properties or corresponding to the objects of interest. The local image properties are described using a feature vector, yielding class probabilities using a learned probability model. Spatial coherence can be imposed e.g. by formulating the segmentation as a discrete labeling problem. In Figure 1a we see the segmentation of red blood cells and detection of malaria parasites [35]; in Figure 1b there are Langerhans islets to be segmented and counted [40]. Figure 1c shows the segmentation results by our

fast-level set method [37], based on quantizing the level set function and discrete evaluation of curvature.

Localization is a special type of segmentation, where we know that a specific object is present and are interested to determine its precise position. We have developed a method to localize a thin needle in 3D ultrasound volume using line filtering, classification, and RANSAC [2], Figure 1d.

2.3 Classification

While segmentation divides an image into regions, classification assigns each of the regions, or the whole image into one of a set of classes which may correspond to, for example, different tissue types or different diagnoses. The decision is often binary, e.g. healthy versus diseased. Standard classification methods from machine learning such as SVM or random forest are used, the challenge is in designing the numerical features describing the image properties in the region being classified. However, it has been shown recently,that if a sufficient amount of training data is available, the features can be determined automatically using e.g. *deep learning* [24].

As an example, consider the task of detecting *lung nodules*, related to lung cancer, from 3D CT volumes [38], Figure 1e. We first quickly detect a number of candidate seed points using blob detection, then segment the neighborhood of each candidate using region growing and calculate a large number of shape and appearance features. Finally, an AdaBoost classifier is employed to prune the non-nodules from the candidate list.

Currently, we work on detecting multiple myeloma from femur CT images (Figure 1e), which is often manifested by higher intensity infiltrations. First, spatially dependent model of healthy tissue intensity is built from a set of data of healthy subjects after registering them onto a common reference. The model is used to detect possible infiltration regions. In the last step, information about all possible infiltrations within a femur are aggregated to arrive at a per-subject decision.

Chapter 3

Image Registration

Image registration finds a coordinate transformation between corresponding points in two given images. Image registration is applied to images of the same subject taken in different times, by different modalities, under different conditions, as well as images of the same region in different subjects. The goal can be to compare or fuse information from these images, as well as obtaining quantitative and qualitative information from the deformation itself. We will take about some of the applications in Chapter 4.

Due to the lack of space, our treatment of the topic here is necessarily going to be incomplete. I will therefore concentrate on the main ideas, giving examples from my own work and the work of my collaborators. There is a vast literature on registration, an interested reader is invited to read for example the surveys [18, 23, 22].

3.1 Registration as minimization

Given two images $f(\mathbf{x})$ and $g(\mathbf{y})$, image registration finds a coordinate transformation $\mathbf{y} = T(\mathbf{x})$ between corresponding points in both images. Most registration algorithms can be described as minimizing a sum of a data criterion J_D and a regularity criterion R with respect to a geometrical transformation T from some class $\mathscr{T}$.

The so-called *moving image* g is deformed by the transformation T, yielding the deformed image $g' = g \circ T$, with $g'(\mathbf{x}) = g\big(T(\mathbf{x})\big)$. The data criterion J_D measures how similar the images g' and f are for a given T and can be often expressed as $J_D = J(f, g')$, leading to a standard formulation of the image registration as a minimization problem

$$T^* = \arg\min_{T \in \mathscr{T}} E(T) \quad \text{with} \quad E(T) = J(f, g \circ T) + R(T) \tag{3.1}$$

It is often useful to assume that the images are real functions of a real argument $f, g : \mathbb{R}^n \to \mathbb{R}^d$. However, in practice digital images are

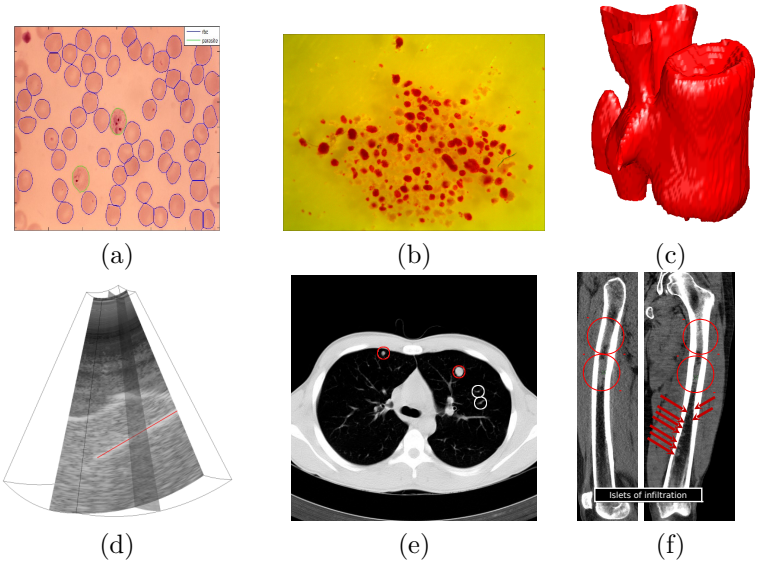

(a) (b) (c) (d) (e) (f)

Figure 1: Biomedical imaging tasks: finding red blood cells and parasites within them (a), counting Langerhans islets (b), 3D segmentation of a vertebra from CT using fast level sets (c), localization of needle in a 3D ultrasound (d), detection of lung nodules from CT (e, true positives in red), detection of myeloma in femurs (f).

both discretized and quantized and the continuous version needed for the deformation is obtained by *interpolation*. Moreover, images are typically only defined in a bounded region of interest Ω, which requires to define *boundary conditions* for arguments (coordinates) outside Ω.

3.2 Deformation function

We shall describe the transformations (or deformation functions) $T \in \mathscr{T}$ by a model parameterized by a finite-dimensional vector $\theta \in \mathbb{R}^N$. One of the simplest examples of transformations (deformation functions) is a 2D rigid transformation, consisting of a rotation and shift

$$T(\mathbf{x}) = \begin{bmatrix} \cos\phi & \sin\phi \\ -\sin\phi & \cos\phi \end{bmatrix} \mathbf{x} + \begin{bmatrix} t_x \\ t_y \end{bmatrix} \tag{3.2}$$

described by a parameter vector $\theta = (\phi, t_x, t_y)$. This transformation is *non-linear* in ϕ and is an example of *global* transformations. Other

transformations are expressed as a linear combination of basis functions $\varphi_i : \mathbb{R}^n \to \mathbb{R}^d$ with coefficients given by the parameter vector θ:

$$T(\mathbf{x}) = \sum_{i=1}^{N} \theta_i \boldsymbol{\varphi}_i(\mathbf{x}) \tag{3.3}$$

Specifically, we have had good results in representing the transformation using *B-splines* [17, 28, 27]

$$T(\mathbf{x}) = \sum_{\mathbf{k}} \mathbf{c}_k \boldsymbol{\beta}_m(\mathbf{x}/\mathbf{h} - \mathbf{k}) \tag{3.4}$$

with $\boldsymbol{\beta}_m$ being a tensor product of B-splines of order m

$$\boldsymbol{\beta}_m(\mathbf{x}) = \prod_{j=1}^{n} \beta_m(x_j/h_j - k_j) \tag{3.5}$$

The B-splines are defined recursively as $\beta_{n+1} = \beta_n * \beta_0$, with β_0 being the Haar function, $\beta_0(x) = [\![|x| < \frac{1}{2}]\!]$. The B-splines are piece-wise polynomial functions of degree n, for example the most often used cubic B-spline is defined as

$$\beta_3(x) = \begin{cases} 2/3 - (1 - |x|/2)x^2 & \text{if } 0 < |x| \leq 1 \\ (2 - |x|)^3/6 & \text{if } 1 < |x| < 2 \\ 0 & \text{otherwise} \end{cases} \tag{3.6}$$

The B-spline representation has a number of advantages: (i) good approximation properties, for β_3 the error decreases as $O(h^4)$; (ii) short support leading to fast algorithms; (iii) can represent polynomials up to degree 3; (iv) coarse to fine transition is exact for integer scale factors.

When additional penalization of unsmooth deformations is needed, we add a *regularization* criterion R, for example the Duchon semi-norm $\|\cdot\|_{D_M}$ [25, 26], which is defined as a sum of the ℓ_2 norms of all possible partial derivatives of T of order M, e.g. for $M = 2$, $n = 2$, $d = 1$:

$$\|f\|^2_{D_2} = \int_{\mathbb{R}^2} \left(\frac{\partial^2 f}{\partial x_1^2}\right)^2 + 2\left(\frac{\partial^2 f}{\partial x_1 \partial x_2}\right)^2 + \left(\frac{\partial^2 f}{\partial x_2^2}\right)^2 \mathrm{d}x_1 \mathrm{d}x_2 \tag{3.7}$$

Regularization is essential when the deformation T is represented in a *non-parametric* and *local* manner, i.e. using the displacement values at the pixels. This is typical for the optical-flow methods [11, 4] which minimize a criterion such as

$$E_{\mathrm{CLG}}(\mathbf{w}) = \int_{\Omega^c} \mathbf{w}^T \left(K_\rho * \left(\nabla_3 \xi \, \nabla_3 \xi^T\right)\right) \mathbf{w} + \alpha \|\nabla \mathbf{w}\|^2 \, \mathrm{d}x \mathrm{d}y$$

where $K_\bullet$ represents a Gaussian kernel, $\xi = K_\sigma * [f; g]$ is a smoothed version of the images f, g considered as a time sequence and $\mathbf{w} = [T(\mathbf{x}) - \mathbf{x}; 1]^T$ represents the deformation field.

In [39], we represent the deformation by a small number of scattered control points $\mathbf{x}_i$, which are triangulated and the regularization penalizes relative control point displacements $\tilde{\mathbf{x}}_i = T(\mathbf{x}_i) - \mathbf{x}_i$

$$R = \gamma \frac{1}{2} \sum_{(i,j)\in\mathscr{E}} \omega_{ij} \|\tilde{\mathbf{x}}_i - \tilde{\mathbf{x}}_j\|^2 \tag{3.8}$$

with weights ω_{ij} set to approximate the behavior of a thin membrane [20]

$$\omega_{ij} = \lambda \frac{\|\mathbf{r}_i - \mathbf{r}_j\|^2}{8A} \left(3 \cot^2 \alpha + \frac{1}{2}\right) \tag{3.9}$$

where λ is the Lamé's first parameter, A is the triangle area and α is the angle oposite to the edge ij.

3.3 Data criterion

In computer vision, it is often possible to identify feature points (landmarks) in both images and find correspondence between them [15]. The data criterion can then be based on the distance between corresponding landmarks $\mathbf{z}_j$ in both images

$$J_D(T) = \sum_j \|\mathbf{z}_j^f - T(\mathbf{z}_j^g)\|^2 \tag{3.10}$$

In medical imaging, this occurs mostly if the landmarks are determined manually. Instead, similarity criteria are used that compare all pixels in both images. An iconic example is the sum of squares (SSD) criterion, here in its discrete form

$$J_{\mathrm{SSD}}(f, g) = \sum_{\mathbf{i}\in\Omega} \|f(\mathbf{i}) - g(\mathbf{i})\|^2 \tag{3.11}$$

which is fast to calculate and corresponds to the ML estimate in case of Gaussian noise. Correlation and normalized correlation are also often used. For *multimodal registration*, the most often used criteria is *mutual information* (MI) [16] and derived measures, with the negative MI defined for quantized and discretized images as

$$J_{\mathrm{MI}}(f, g) = -\sum_{k,l} p_{k,l} \log \frac{p_{k,l}}{p_k p_l} \tag{3.12}$$

with $p_k = \sum_l p_{k,l}$ and $p_l = \sum_k p_{k,l}$, where $p_{k,l}$ is a probability that for random $\mathbf{i} \in \Omega$ we have $f(\mathbf{i}) = k$ and $g(\mathbf{i}) = l$. The mutual information can be also written as a difference of entropies:

$$J_{\mathrm{MI}}(f, g) = H(f, g) - H(f) - H(g) \tag{3.13}$$

Standard MI assumes that the joint pdf $p_{k,l}$ is the same everywhere. If this is not true, we suggest to augment the criterion by using a segmentation L [9] to obtain *organ-focused MI*

$$J_{\mathrm{OFMI}}(f, L, g) = H(f, g, L) - H(f, L) - H(g) \tag{3.14}$$

which improves the results for example for contrast enhanced images.

In another work, we have shown that the MI can be applied on the segmented images which leads to improvement of speed and robustness but almost no loss of registration accuracy [39].

Going in the other direction, we might wish to apply MI to vector images, for example to apply it to color images, or to feature vectors capturing local image properties and thus increasing the specificity of the matching. Unfortunately, standard histogram estimator or kernel density estimator perform poorly in higher dimensions e.g. due to binning. We have therefore used a little known Kozachenko-Leonenko nearest neighbor (NN) distance based entropy estimator which is more suitable for high dimensional data

$$H(\mathbf{U}) = \frac{d}{n} \sum_{\mathbf{u}_i} \log \rho_{\mathbf{u}_i} + \log \frac{(n-1)\pi^{d/2}}{\Gamma(1 + d/2)} + \gamma_e \tag{3.15}$$

where $\mathbf{U}$ is a random variable on $\mathbb{R}^d$ with samples $\mathbf{u}_i$, $\varrho_{\mathbf{u}_i}$ is the distance from $\mathbf{u}_i$ to its nearest neighbor. We have succesfully used the MI criterion calculated using (3.15) and a feature vector consisting of pixels from a small neighborhood to register colour colposcopy images [5]. As the computational bottleneck is the all-NN search, we have developed a specialized approximative k-d tree-based all-NN search algorithm with several improvements, tailored to this problem [6], which outperformed other approaches available.

3.4 Optimization

If the transformation T is represented by a finite-dimensional parameter vector $\theta \in \mathbb{R}^N$, the registration criterion (3.1) can be minimized by standard iterative multidimensional optimization techniques. We have succesfully used the Marquardt-Levenberg-like modification of the

Newton's method [28]

$$-\big(\nabla^2 E(\theta) + \lambda \mathsf{I}\big)\Delta\theta = \nabla_\theta E(\theta) \tag{3.16}$$

where $\Delta\theta = \theta^{(t)} - \theta^{(t-1)}$ is the increment of θ in successive iterations. Thich works best for low N. For higher N, it is better to avoid the computational cost of evaluating the second derivatives by using the conjugated gradient method, the L-BFGS method, or even the derivative-less NEWUOA method [5]. As most time is spent far from the optimum, a simple gradient descent [27]

$$\Delta\theta = -\lambda \nabla_\theta E(\theta) \tag{3.17}$$

with automatic control of the step size λ is often the fastest method. Further acceleration can be obtained by using only a random subset of the pixels [14].

We have obtained a fast algorithm by considering only small regions around the class boundaries [39] and representing the data criterion as a sum of contributions D_i from small patches around control points $\mathbf{x}_i$

$$J_D = \sum_{\mathbf{x}_i} D_i\big(\underbrace{T(\mathbf{x}_i) - \mathbf{x}_i}_{\tilde{\mathbf{x}}_i}\big) \tag{3.18}$$

The sum of the patch-based data criterion (3.18) and the control point regularization (3.8) is optimized by allowing only quantized (integer) displacements $T(\mathbf{x}_i)$. This leads to a discrete labeling problem, which can be solved efficiently using min-convolution and message passing [13], which sends messages

$$\mu^t_{i\to j}(\tilde{\mathbf{x}}_j) = \min_{\tilde{\mathbf{x}}_i}\Big(\frac{\omega_{ij}}{2}\|\tilde{\mathbf{x}}_i - \tilde{\mathbf{x}}_j\|^2 + D_i(\tilde{\mathbf{x}}_i) + \sum_{s\neq j} \mu^{t-1}_{s\to i}(\tilde{\mathbf{x}}_i)\Big) \tag{3.19}$$

between neighboring nodes until convergence. Then the estimated displacement is extracted as $\mathbf{y}^*_j = \arg\min_{\tilde{\mathbf{x}}_j}\big(D_j(\tilde{\mathbf{x}}_j) + \sum_i \mu^t_{i\to j}(\tilde{\mathbf{x}}_j)\big)$.

There are a few special registration methods, where the optimal transformation parameters can be determined in a closed form, a typical example is a Fourier method based on a comparison of phases.

For the optical-flow, when T is represented by individual pixel displacement, the variational criterion is optimized by solving linearized Euler-Langrange equations by successive over-relaxation (SOR).

The speed and robustness of all optimization methods can be improved by a coarse to fine *multiresolution strategy*.

Chapter 4

Image Registration Applications

Let us mention several applications of image registration I have developed in the past. The first is *deformation compensation* for EPI MRI [28], Figure 2a. Local magnetic field inhomogeneities cause significant geometrical distortion in EPI images, which need to be undone for example to accurately localize functional centers identified by fMRI for surgical treatment of epilepsy. The deformation is compensated by registering EPI to anatomical images using B-spline transformation.

The same algorithm can be used to align 3D CT data (Figure 2b). Applying the B-spline method to the *registration of sequences* from ultrasound examination of the heart [31] (Figure 2c) required extending the model (3.4) by the temporal dimension. The temporal basis functions are linear combinations of B-splines, chosen according to our a priori knowledge of the transformation field, namely that the motion is periodic and the displacement is zero at $t = 0$. A similar 3D+time technique was used to register preoperative 3D CT time sequences of the lungs [3, 7] in order to build a low dimensional model of the breathing motion, This permits to estimate the tumor position based on the respiration or cone-beam data taken during acquisition (Figure 2d).

Ultrasound hand-held *elastography* aims to recover the elastic properties of tissue by solving the inverse problem from the estimated tissue movement due to a probe pressure [34], Figure 2e. Image registration is a crucial component of the pipeline as the motion needs to be precisely estimated, in this case from the RF (raw) signal. We chose an application specific dense representation of the deformation (axial scaling factor and lateral shift) with regularization, optimized using quadratic programming with problem-specific constraints (e.g. zero displacement at the probe boundary).

The *motion compensation* of colposcopy sequence images [5] was challenging because of the color changes during the sequence (Fig-

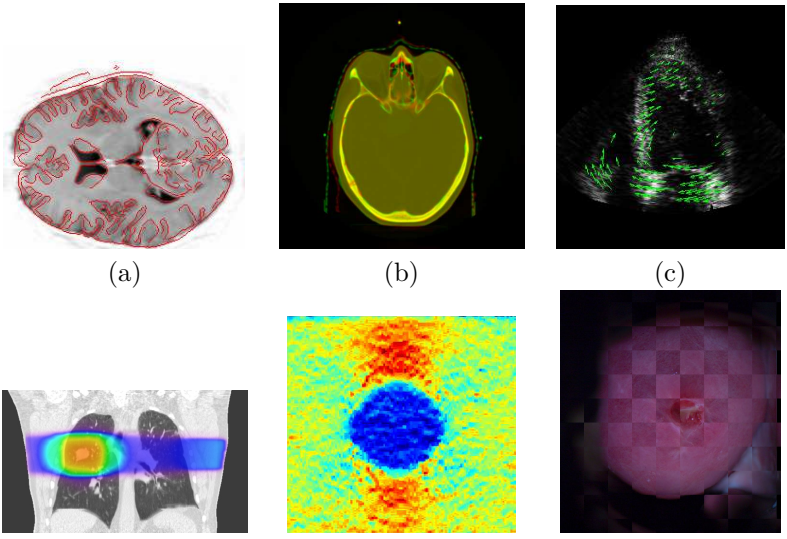

(a) (b) (c)

(d) (e) (f)

Figure 2: Image registration examples: Deformation corrected MRI EPI image with edges from the anatomical MRI image overlaid (a). One slice of two 3D CT volumes shown overlaid in green and red before after registration (a), yellow corresponds to perfect overlap (b). Heart motion estimation from ultrasound sequence registration (c). Breathing motion model for radiation therapy, estimated dose (d). Estimated axial strain from ultrasound elastography on a phantom (f). Colposcopy sequence — reference and moving images superimposed using a checkerboard patte ern (e).

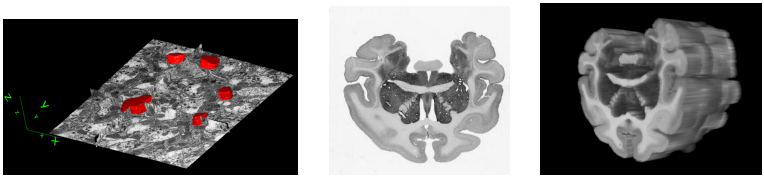

(a) (b) (c)

Figure 3: Reconstructed cells in 3D from a sequence of transmission electron microscopy images (a). One brain histological section (b) and the resulting 3D reconstruction (c).

ure 2f). This required the use of a high dimensional Mutual information criterion, as explained in Section 3.3. Dual compartment model parameters are then fitted in each pixel of the motion compensated sequence and classified using SVM to detect abnormalities.

The task of registering *histological slices* [1] (Figure 3) required deformations to be modeled separately, as the transformations are not likely to be correlated. Due to the high number of images to be registered, it would not be feasible to optimize all transformations simultaneously anyway. We consider triples of images f_{i-1}, f_i, f_{i+1} and for each triple we simultaneously optimize the four transformations $T_{i-1,i}$, $T_{i,i-1}$, $T_{i,i+1}$, and $T_{i+1,i}$, while enforcing their consistency. Successive triples of images from the sequence are iteratively registered forward and backward until convergence. This algorithm is available in Fiji [1].

[1] `http://fiji.sc/wiki/index.php/Register_Virtual_Stack_Slices`

Chapter 5

Extensions and current work

5.1 Error estimation

Most image registration algorithms return just a single, deterministic answer, a point-wise estimate of the unknown geometric transformation. However, in practice there is always some associated uncertainty, the registration accuracy is limited. Knowing this uncertainty is useful to determine whether and to what extent the registration results can be trusted and whether the input data is suitable. We have developed a method of estimating the registration result uncertainty, which does not need the ground truth [36].

Bootstrap resampling [12] (Figure 4) is a computational technique for assessing the accuracy of a parametric estimator in small sample situations, based on randomly selecting samples with replacement from the original dataset of the same size. In our case, the boostrap constructs a multiset S from the set of all pixels of interest Ω, which yields a bootstrap version of the data criterion J_D, which is then optimized to find the bootstrap result $T^{(b)}$. The statistics of the bootstrap run results approximates the unknown statistics of the true results T^* across realizations. Later on we have extended the same approach to optical flow [4].

5.2 Geometric graph matching

Blood vessels, nerve fibers or pulmonary airways are examples of biological structures that can be represented as *geometrical graphs* with nodes corresponding to branching points and edges corresponding to curves connecting the branching points (Figure 5). We suggest to register images containing such graphs by first matching the graphs and then interpolating and extrapolating the deformation field everywhere [10]. This has the potential of being much faster than standard pixel-based im-

age registration techniques (Chapter 3), being applicable to very large images and tolerate very different image appearances. We consider the case where a good initial guess of the transformation is not available and at the same time there is important non-linear transformation between the two graphs, which makes the problem very challenging and prevents existing methods such iterative closest points [41], Coherent Point Drift [44] or spectral graph matching [43].

In the first, coarse matching phase, the branching points are matched. We use a Gaussian process model of the deformation field. Given a set of corresponding coordinates of already matched points in both graphs, and a query point in one graph, we can calculate the expected location and uncertainty region of the matching point in the other graph (the ellipses in Figure 6) and thus prune many possible matches. In the simplest case, the matching proceeds in a greedy manner, adding matching point pairs using a simple heuristics as long as possible, with backtracking (Figure 6).

A significant speed-up can be obtained by replacing the heuristics with *active test search*, which guides the search by estimating the probability of a current partial match to be part of the optimal solution. The probability is estimated from a number of features, such as the residual error and the number of inliers. The probability model is learned from training data. Active learning had a significantly lower computational cost than the alternatives tested (Figure 7a).

The coarse matching can also be formulated as a *single player game*. In each step, the player can add one pair of matching edges (or so-called superedges, in order to allow for missing nodes) as long as they are consistent with the current partial match. The player's objective is to maximize the weighted sum of the length of matched edges and the number of matched vertices. The game is solved by a search algorithm inspired by the Upper Confidence Bound on Trees (UCT), a variant of the *Monte Carlo Tree Search* (MCTS) [45]. The algorithm balances between exploration of the search space (of partial matches) and exploitation (improving) the best solutions found so far. In each iteration, an expandable search space node ν with the highest urgency $\tilde{Q}_\nu$ is selected by a greedy top-down search, with

$$\tilde{Q}_\nu = \frac{Q^+_\nu}{Q_{\text{norm}}} + \gamma\sqrt{\frac{2\log n}{n_\nu}}. \tag{5.1}$$

where Q^+_ν is our estimate of the best criterion value obtainable by expanding node ν. The node is expanded, Q^+ values updated and the process is repeated until the computational budget is exhausted.

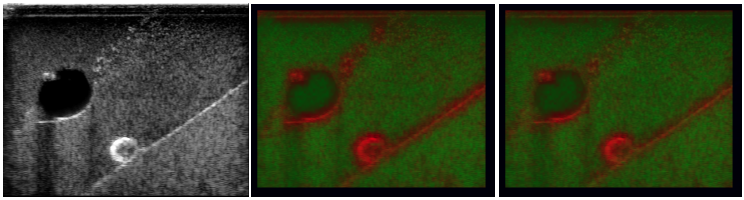

(a) (b) (c)

Figure 4: Reference image (a), true registration error (b) and bootstrap estimation of the registration error (c), with red meaning low uncertainty and green corresponding to high uncertainty. (Best viewed in color.)

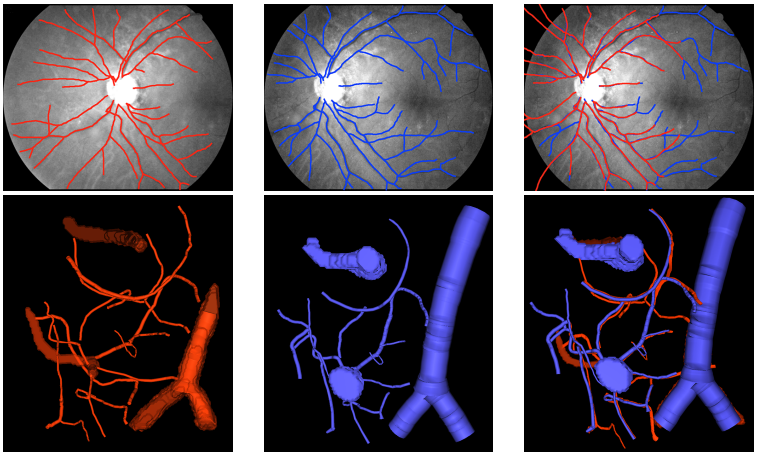

(a) (b) (c)

Figure 5: Geometric graph matching results. **(a)** and **(b)** are the original images or structures, with extracted graphs. **(c)** is the obtained alignment. Top row shows 2D images of vessels in human retina, bottom row are 3D images of axons and blood vessels in brain tissue from the two-photon microscopy.

Once the branching points are matched, the edges between them are matched using fine alignment (Figure 7bc) based on solving the assignment problem between the edge points using the Hungarian algorithm, using the geometric residual error as a matching quality criterion.

5.3 Segmentation and registration

For many image registration tasks, there is not enough information to determine correspondence of all individual pixels and it is therefore

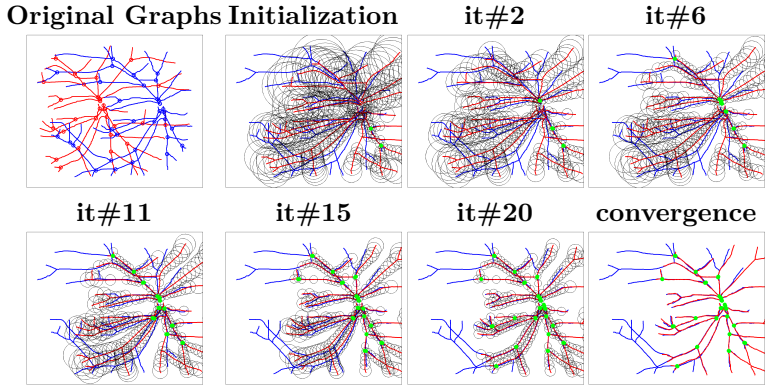

Figure 6: Coarse alignment steps of the graph matching algorithm between the red and blue graphs. The correspondences found are in green, the black ellipses denote uncertainty regions. Best viewed in color.

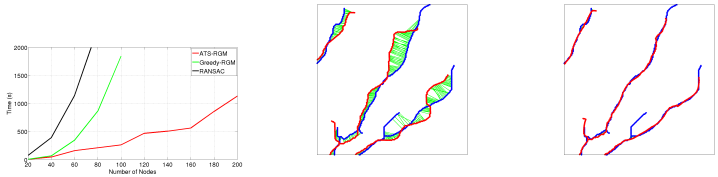

(a) (b) (c)

Figure 7: Comparison of computation cost for graph matching (a). Detail of the graphs before (b) and after (c) fine registration, with the two graphs in red and blue, and the green lines connecting corresponding points.

a waste of computational effort to use all pixels. Often, we are able to match only edges and the transformation elsewhere is interpolated. Hence, we suggest that the images are first segmented into a small number of classes and then the registration is performed considering only a sparse set of rectangular windows on the boundary between classes [39]. The unique feature of our approach is that segmentation and registration is solved jointly, by minimizing a common criterion, a negative *mutual information on labels* $J_{\mathrm{MI}}(f, g \circ T)$ from (3.12) where this time $p_{k,l}$ is the probability of observing *classes* k,l in corresponding pixels of the soft segmentations $f = \Psi_f F$, $g = \Psi_g G$, and F,G are the original images.

For the segmentation of both images, we use a softmax regres-

method	time	mean err.	median err.	success rate
bUnwarpJ	401	64	50	50%
Elastix	515	54	45	67%
OpenCV+Elastix	764	23	12	88%
ASSAR	130	36	17	91%

Table 5.1: Comparison of registration methods. We show the execution time in seconds, the mean and median registration error in pixels, and percentage of successful runs.

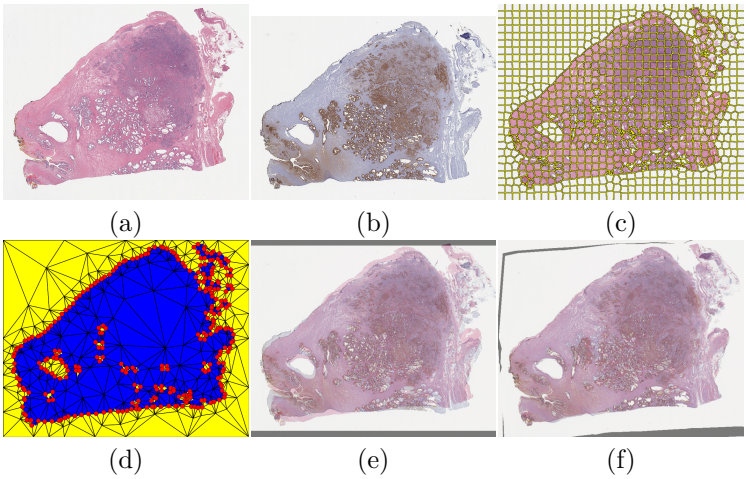

Figure 8: Histology slices of human prostate stained with H&E (a) and PSAP (b), superpixels (c), the segmentation and the triangulated mesh (d), overlaid images before (e) and after (f) registration.

sion [42], in this case linear:

$$f_k(i) = \frac{\exp\left(\mathbf{a}_k^T \mathbf{u}_i\right)}{\sum_{l=1}^{L} \exp\left(\mathbf{a}_l^T \mathbf{u}_i\right)} \tag{5.2}$$

Softmax converts local image features $\mathbf{u}_i$ into probabilities $f_k(i)$ for each class k. For further speedup, the classification is performed on SLIC superpixels [19]. The image specific coefficients $\mathbf{a}_k$ are found using L-BFGS.

The registration is performed by representing the deformation by a sparse set of control points and optimizing their displacement using message passing as described in Section 3.4. Registration and segmentation are iteratively updated until convergence and multiresolution is also used to improve speed and robustness.

The transformation T is then evaluated everywhere using bilinear interpolation or the Clough-Tocher scheme [21], if more smoothness is required.

Figure 8 shows the results for differently stained nearby histological slices of human prostate of about 2000×2000 pixels. Our results on a dataset of 34 histology images with manually identified landmarks (Table 5.1) show that our method has the highest success rate among all tested methods and it is also the fastest.

We are currently working on approximating the criterion by sampling the moving image only on a short straight line perpendicular to the boundary, which decreases the registration time by another order of magnitude.

Chapter 6

Conclusions and challenges

Image registration is a necessary part of most image analysis methods that analyze more than one image at a time. It is needed for many tasks, such as motion compensation, deformation compensation, image fusion, motion analysis, time evolution analysis, change detection, comparison between subjects, atlas creation and use, and many others. It is a mature filed of research with many thousands of publications. This is even more true for the whole field of biomedical imaging, which has a number of very prestigious scientific journals (such as *IEEE Transactions on Medical Imaging* or *Medical Image Analysis*) and a number of good conferences (MICCAI, ISBI, IPMI). Most computer vision and image processing conferences (CVPR, ICCV, ECCV, ICIP) now also accept papers about biomedical image processing.

Despite the number of available methods, image registration is by far not a solved problem. There is no single registration method that would work for all data and new methods are constantly being developed, aiming to improve the speed, robustness or accuracy of existing methods. Of particular interest are methods capable of processing very large number of images automatically, without human intervention.

The task of image registration is easy to understand intuitively but there are many variants of possible mathematical formulations that the researcher needs to select from when faced with the task of registering a given type of image data. Most of these formulations lead to complicated high-dimensional non-linear problems, for which increasingly more sophisticated algorithms are developed.

We have not approached the issue of image registration validation, which is notoriously difficult, because creating ground truth data is very labor-intensive. This is slowly starting to change, with several datasets suitable for image registration algorithm evaluation now available.

The main purpose of this work was to give the reader an idea about

the task of image registration, the purpose, the problems and the methods employed. We have also talked briefly about other important tasks in biomedical image processing.

The secondary purpose was to present, at least partially, my own contribution to the area. A lot of this work was done by my PhD students and postdocs at CTU Prague, or in collaboration with my colleagues from EPFL Lausanne, UPM Madrid, INSA Lyon, University of Heidelberg and others.

6.1 Perspectives and education

I see a great future and opportunity in biomedical image processing. As the population ages, the need for medical care and thus medical imaging will increase. In biology, large throughput methods produce images in quantities which are impossible to analyze manually. Funding agencies such as the National Institute of Health in the U.S.A. devote a large part of their budget to biomedical imaging.

Many good universities now have a master-level programme related to biomedical imaging. A number of top universities (such as Johns Hopkins University or University College London) also have PhD-level programmes. So far, CTU lags in this aspect, even behind other Czech Universities, such as VUT or Masaryk University in Brno. At CTU, there is very little research done in the area of biomedical imaging and biomedical image analysis and there is no possibility for students to learn the related techniques. Improving this situation is a worthy long term goal. I am willing to help fulfilling this goal as far as my humble forces allow.

6.2 Future activities

I do not expect my research direction to change dramatically. I will continue to focus on developing methods and algorithms for biomedical imaging. I will be actively looking for funding and collaborations especially with our clients and data providers, clinicians and biologists. The size of my team should increase but not at the expense of quality.

As far as teaching is concerned, in the future I would like to teach a course on advanced algorithms for biomedical image processing and analysis. Combined with already existing courses such as Optimization, Image Processing, Machine Learning, or Medical Imaging Devices, this should give our master students a suitable background knowledge for a future research in the industry or PhD studies in this field.

doc. Dr. Ing. Jan Kybic

Born on 18^{th} January 1974 in Prague, Czech Republic.

`http://cmp.felk.cvut.cz/~kybic`

Academic appointments

since 2013 **Head of the Department of Cybernetics**, *Faculty of Electrical Engineering (FEE)*, Czech Technical University in Prague (CTU).

2011–2013 **Vice-dean for information technology**, *Faculty of Electrical Engineering (FEE)*, Czech Technical University in Prague (CTU).

since 2011 **Associate professor (doc.)**, *FEE*, CTU.

since 2003 **Senior researcher**, *Center for Machine Perception, Department of Cybernetics, FEE*, CTU.
leading a small research group

2001–2003 **Post-doc**, *INRIA*, Sophia-Antipolis, France, with Olivier Faugeras.
working on inverse problems in MEG and EEG

Education

1998–2001 **PhD**, *EPFL*, Lausanne, Switzerland, with Michael Unser.
thesis *Elastic Image Registration using Parametric Deformation Models*

1994–1998 **Master *(Ing.)***, *FEE*, CTU.
thesis *Kalman Filtering and Speech Enhancement*

1994–1996 **Bachelor *(Bc.)***, *FEE*, CTU.
thesis *Programming Contest Scoring System*

Journal publications (2010–2015)

[1] I. Arganda-Carreras, C. O. S. Sorzano, P. Thévenaz, A. Muñoz-Barrutia, J. Kybic, R. Marabini, J. M. Carazo, and C. Ortiz-de Solorzano, "Non-rigid consistent registration of 2D image sequences," *Physics in Medicine and Biology*, vol. 55, no. 20, pp. 6215–6242, Sept. 2010.

[2] Marián Uherčík, Jan Kybic, Hervé Liebgott, and Christian Cachard, "Model fitting using RANSAC for surgical tool localization in 3-D ultrasound images," *IEEE Transactions on Biomedical Engineering*, vol. 57, no. 8, pp. 1907–1916, Aug. 2010.

[3] J. Vandemeulebroucke, S. Rit, J. Kybic, P. Clarysse, and D. Sarrut, "Spatio-temporal motion estimation for respiratory-correlated imaging of the lungs," *Medical Physics*, vol. 38, no. 1, pp. 166–178, 2011.

[4] Jan Kybic and Claudia Nieuwenhuis, "Bootstrap optical flow confidence and uncertainty measure," *Computer Vision and Image Understanding*, vol. 115, no. 10, pp. 1449–1462, June 2011.

[5] Juan David García-Arteaga, Jan Kybic, and Wenjing Li, "Automatic colposcopy video tissue classification using higher order entropy based registration," *Computers in Biology and Medicine*, vol. 41, no. 10, pp. 960–970, Oct. 2011.

[6] Jan Kybic and Ivan Vnučko, "Approximate all nearest neighbor search for high dimensional entropy estimation for image registration," *Signal Processing*, vol. 92, no. 5, pp. 1302–1316, 2012.

[7] J. Vandemeulebroucke, O. Bernard, S. Rit, J. Kybic, P. Clarysse, and D. Sarrut, "Automated segmentation of a motion mask to preserve sliding motion in deformable registration of thoracic CT," *Medical Physics*, vol. 39, no. 2, pp. 1006–1015, 2012.

[8] Marian Uhercik, Jan Kybic, Yue Zhao, Christian Cachard, and Herve Liebgott, "Line filtering for surgical tool localization in 3D ultrasound images," *Computers in Biology and Medicine*, vol. 43, no. 12, pp. 2036–2045, Dec. 2013.

[9] L. Fernandez-de Manuel, G. Wollny, J. Kybic, Daniel Jimenez-Carretero, Jose M. Tellado, E. Ramon, M. Desco, A. Santos, J. Pascau, and M. Ledesma-Carbayo, "Organ-focused mutual information for non-rigid multimodal registration of liver CT and Gd-EOB-DTPA-enhanced MRI," *Medical Image Analysis*, vol. 18, no. 1, pp. 22–35, Jan. 2014.

[10] Eduard Serradell, Miguel Amável Pinheiro, Raphael Sznitman, Jan Kybic, Francesc Moreno-Noguer, and Pascal Fua, "Non-rigid graph registration using active testing search," *IEEE Transactions on Pattern Analysis and Machine Intelligence*, vol. 37, no. 3, pp. 625–638, Mar. 2015.

See `http://cmp.felk.cvut.cz/~kybic` for a complete list of publications.

Other references

[11] Andrés Bruhn, Joachim Weickert, and Christoph Schnörr, "Lucas/Kanade meets Horn/Schunck: combining local and global optic flow methods," *Int. J. Comput. Vision*, vol. 61, no. 3, pp. 211–231, 2005.

[12] B. Efron and R. Tibshirani, *An Introduction to the Bootstrap*, Number 57 in Monographs on Statistics and Applied Probability. Chapman & Hall, CRC, 1993.

[13] Pedro F. Felzenszwalb and Daniel P. Huttenlocher, "Efficient belief propagation for early vision," *International Journal of Computer Vision*, , no. 1, pp. 41–54, Oct. 2006.

[14] Stefan Klein, Marius Staring, and Josien P.W. Pluim, "Evaluation of optimization methods for nonrigid medical image registration using mutual information and B-splines," *IEEE Transactions on Image Processing*, vol. 16, no. 12, pp. 2879–2890, Dec. 2007.

[15] D. Lowe, "Distinctive image features from scale-invariant keypoints," *International Journal of Computer Vision*, vol. 60, no. 2, pp. 91–110, 2004.

[16] J.P.W. Pluim, J. B. A. Maintz, and M. A. Viergever, "Mutual-information-based registration of medical images: A survey," *IEEE Transactions on Medical Imaging*, vol. 22, no. 8, pp. 986–1004, Aug. 2003.

[17] Michael Unser, "Splines: A perfect fit for signal and image processing," *IEEE Signal Processing Magazine*, vol. 16, no. 6, pp. 22–38, Nov. 1999.

[18] Barbara Zitová and Jan Flusser, "Image registration methods: a survey," *Image and Vision Computing*, , no. 21, pp. 977–1000, 2003.

[19] R. Achanta, A. Shaji, K. Smith, A. Lucchi, P. Fua, and S. Süsstrunk, "Slic superpixels compared to state-of-the-art superpixel methods," *Pattern Analysis and Machine Intelligence, IEEE Transactions on*, vol. 34, no. 11, pp. 2274–2282, nov. 2012.

[20] H. Delingette, "Triangular springs for modeling nonlinear membranes," *IEEE Transactions on Visualization and Computer Graphics*, vol. 14, no. 2, 2008.

[21] R. W. Clough and J. L. Tocher, "Finite element stiffness matrices for analysis of plates," in *Proceedings of the conference on matrix methods in structural mechanics*, 1965.

[22] Lisa Tang and Ghassan Hamarneh, "Medical image registration: A review (Chapter 22)," *Medical Imaging: Technology and Applications*, pp. 619–660, 2013.

[23] A. Sotiras, C. Davatzikos, and N. Paragios, "Deformable Medical Image Registration: A Survey," *Medical Imaging, IEEE Transactions on*, vol. 32, no. 7, pp. 1153–1190, July 2013.

[24] Dan Claudiu Ciresan, Alessandro Giusti, Luca Maria Gambardella, and Jürgen Schmidhuber, "Mitosis detection in breast cancer histology images with deep neural networks," in *MICCAI*, 2013, vol. 2, pp. 411–418.

[25] Jan Kybic, Thierry Blu, and Michael Unser, "Generalized sampling: A variational approach. Part I — Theory," *IEEE Transactions on Signal Processing*, vol. 50, no. 8, pp. 1965–1976, August 2002.

[26] Jan Kybic, Thierry Blu, and Michael Unser, "Generalized sampling: A variational approach. Part II — Applications," *IEEE Transactions on Signal Processing*, vol. 50, no. 8, pp. 1977–1985, August 2002.

[27] Jan Kybic and Michael Unser, "Fast parametric elastic image registration," *IEEE Transactions on Image Processing*, vol. 12, no. 11, pp. 1427–1442, November 2003.

[28] Jan Kybic, Philippe Thévenaz, Arto Nirkko, and Michael Unser, "Unwarping of unidirectionally distorted EPI images," *IEEE Transactions on Medical Imaging*, vol. 19, no. 2, pp. 80–93, February 2000.

[29] Jan Kybic, Maureen Clerc, Touffic Abboud, Olivier Faugeras, Renaud Keriven, and Théo Papadopoulo, "A common formalism for the integral formulations of the forward EEG problem," *IEEE Transactions on Medical Imaging*, vol. 24, no. 1, pp. 12–28, Jan. 2005.

[30] Jan Kybic, Maureen Clerc, Olivier Faugeras, Renaud Keriven, and Théo Papadopoulo, "Generalized head models for MEG/EEG: BEM beyond nested volumes," *Physics in Medicine and Biology*, vol. 51, no. 5, pp. 1333–1346, Feb. 2006, doi:10.1088/0031-9155/51/5/021.

[31] María Jesús Ledesma-Carbayo, Jan Kybic, Manuel Desco, Andrés Santos, Michael Sühling, Patrick Hunziker, and Michael Unser, "Spatio-temporal non-rigid registration for ultrasound cardiac motion estimation," *IEEE Transactions on Medical Imaging*, vol. 24, no. 9, pp. 1113–1126, Sept. 2005.

[32] Jan Kybic, Maureen Clerc, Olivier Faugeras, Renaud Keriven, and Théo Papadopoulo, "Fast multipole acceleration of the MEG/EEG boundary element method," *Physics in Medicine and Biology*, vol. 50, no. 19, pp. 4695–4710, October 2005.

[33] Jan Petr, Jan Kybic, Michael Bock, Sven Müller, and Václav Hlaváč, "Parallel image reconstruction using B-spline approximation (PROBER)," *Magnetic Resonance in Medicine*, vol. 58, no. 9, pp. 582–591, September 2007.

[34] Elisabeth Brusseau, Jan Kybic, Jean-François Déprez, and Olivier Basset, "2-D locally regularized tissue strain estimation from radio-frequency ultrasound images: Theoretical developments and results on experimental data," *IEEE Transactions on Medical Imaging*, vol. 27, no. 2, pp. 145–160, Feb. 2008.

[35] Vít Špringl, "Automatic malaria diagnosis through microscopy imaging," M.S. thesis, Center for Machine Perception, K13133 FEE Czech Technical University, Prague, Czech Republic, Feb. 2009.

[36] Jan Kybic, "Bootstrap resampling for image registration uncertainty estimation without ground truth," *IEEE Trans. Image Processing*, vol. 19, no. 1, pp. 64–73, Jan. 2010.

[37] Jan Kybic and Jakub Krátký, "Discrete curvature calculation for fast level set segmentation," in *ICIP: International Conference on Image Processing*, 445 Hoes Lane, Piscataway, NJ, U.S.A., Nov. 2009, p. 4404, Institute of Electrical and Electronics Engineers, electronic version.

[38] Martin Dolejší, Jan Kybic, Michal Polovinčák, and Stanislav Tůma, "The Lung TIME—Annotated lung nodule dataset and nodule detection framework," in *Proceedings of SPIE*, Maryllen L. Giger and Nico Karssemeijer, Eds., Bellingham, WA, USA, February 2009, vol. 7260 of *Medical Imaging 2009: Computer-Aided Diagnosis*, p. 72601U, SPIE.

[39] Jan Kybic and Jiri Borovec, "Automatic simultaneous segmentation and fast registration of histological images," in *International Symposium on Biomedical Imaging (ISBI)*. April–May 2014, pp. 774–777, IEEE.

[40] J. Švihlík, J. Kybic, D. Habart, Z. Berková, P. Girman, J. Kříž, and K. Zacharovová, "Classification of microscopy images of Langerhans islets," in *Medical Imaging 2014: Image Processing*, Martin A. Styner Sebastien Ourselin, Ed., Bellingham, Washington, March 2014, SPIE, vol. 9034, pp. 1–8, SPIE.

[41] Paul J. Besl and Neil D. McKay, "A method for registration of 3-D shapes," *IEEE Transactions on Pattern Analysis and Machine Intelligence*, vol. 14, no. 2, pp. 239–256, Feb. 1992.

[42] T. Hastie, R. Tibshirani, and J. Friedman, *The Elements of Statistical Learning*, Springer, 2001.

[43] M. Leordeanu and M. Hebert, "A Spectral Technique for Correspondence Problems Using Pairwise Constraints," in *International Conference on Computer Vision*, October 2005, pp. 1482–1489.

[44] A. Myronenko and X.B. Song, "Point-Set Registration: Coherent Point Drift," *IEEE Transactions on Pattern Analysis and Machine Intelligence*, vol. 32, no. 12, pp. 2262–2275, 2010.

[45] Cameron Browne, Edward J. Powley, Daniel Whitehouse, Simon M. Lucas, Peter I. Cowling, Philipp Rohlfshagen, Stephen Tavener, Diego Perez, Spyridon Samothrakis, and Simon Colton, "A survey of Monte Carlo tree search methods," *IEEE Trans. Comput. Intellig. and AI in Games*, vol. 4, no. 1, pp. 1–43, 2012.